Multiple resonance in coupled Duffing oscillators and nonlinear normal modes

Rosty B. Martinez Duque [1,*] and Carlos E. Vásquez Romero [2,†]
[1]*Physics Department, Oklahoma State University, Stillwater, Oklahoma 74075, USA*
[2]*Departamento de Física, Universidad Simón Bolívar, Apartado 89000, Caracas 1080-A, Venezuela*

(Received 25 September 2023; accepted 29 March 2024; published 26 April 2024)

The resonance of N linearly coupled damped Duffing oscillators with a constant frequency sinusoidal driving force acting on the first oscillator is studied analytically by calculating the fixed points of the corresponding dynamical system and numerically using a fourth-order multivariate Runge-Kutta method. For a chain with N oscillators, we establish a general recursion scheme in the form of a system of equations that relates the amplitudes of the oscillators and the driving frequency, capable of describing resonance curves. We consider in detail the case of an oscillator chain with $N = 2$ for high values of the driving amplitude and stiffness, and find hysteretical unstable regions in the resonance curves. In this unstable driving frequency regime, analysis of the time series reveals the presence of nonlinear normal modes visible as beating quasiperiodic oscillations.

DOI: 10.1103/PhysRevE.109.044216

I. INTRODUCTION

Linear dynamics started as a branch of physics that studied problems such as planetary motion, but with the need to describe more complex systems, e.g., Newton's three-body problem, this field evolved to an interdisciplinary subject that incorporates more sophisticated concepts, such as nonlinear oscillations, fractals, turbulence, and chaos [1]. Most of these concepts are tied to differential equations and techniques to obtain information about the system from them, such as Poincaré maps, bifurcation diagrams, phase space portraits, Lyapunov exponents, etc. [1–3]. One popular example that exhibits a broad variety of dynamical behaviors is the Duffing equation, which describes an oscillator with a cubic nonlinearity related to the stiffness of the system [4,5]. Nonlinear oscillations can be characterized with the aid of the Duffing equation, describing a plethora of oscillating systems in nature and allowing practical applications, such as in metamaterials [6,7], pure-electron plasmas [8], turbomachinery blades [9], magnetically driven oscillations [10], micromechanical devices [11], vibrations in carbon nanotubes [12], nonlinear vibration energy harvesting [13], signal detection [14], and oscillations in beams and nanobeams [15,16]. In particular, coupled oscillators under the influence of injection and energy dissipation produce complex dynamics that resemble the behavior of flexible structures with local stiffness nonlinearities [17], such as synchronization, spatiotemporal intermittency, defects and/or phase turbulence, defect-mediated turbulence, chimera states, and others [18,19].

The characterization and identification of nonlinear systems is still a new field in development. Techniques like nonlinear system identification (NSI) and reduced order modeling (ROM) have been proposed [20,21], however, they could be limited for some applications [17]. One way to interpret a wide class of nonlinear dynamical phenomena is through the analysis of its nonlinear normal modes (NNMs) [22,23]. NNMs are described with different approaches defining them as an extension of linear normal modes (LNMs) through limiting phase trajectories, modal lines, or invariant manifolds in the phase space [6,9,12,22,24–28]. In this work we will follow the definition of NNMs provided by Haller *et al.* [24], where a NNM is defined as a set filled with small-amplitude recurrent motions such as a fixed point, a periodic orbit, or the closure of a quasiperiodic orbit. Unlike when a system is near resonance with LNMs, under NNMs the motion is not necessarily synchronous but still periodic or quasiperiodic.

We study a chain of N linearly coupled damped Duffing oscillators with a sinusoidal driving force acting on the first oscillator through analytical and numerical methods. This system resembles the oscillation of a cantilever beam by adding a nonlinear stiffness element [17]. Also, it has been implemented by an analog electronic circuit simulation when $N = 2$, obtaining resonance curves that follow the theory prediction [29]. We develop an analytical general solution for this system based on a recursion formula obtained from solving the fixed point equations. In addition, we explore the effects of large values of stiffness and amplitudes in the resonance curves of a chain of two oscillators which produces hysteresis and significant distortions in the second peak of resonance of both oscillators.

For $N = 2$ oscillators, we identify NNMs in the form of quasi-periodic beating responses in the time series at forcing frequencies corresponding to the hysteretic regions of the resonance curve. Notably, even with just two linearly coupled Duffing oscillators, the obtained NNMs' behavior in the amplitude time series is similar to what has already been reported and characterized for a linear cantilever beam attached to ground through a strongly nonlinear stiffness at its free boundary [17], premixed flames [30], and a ring of Duffing oscillators [31], which show strongly nonlinear beats that resemble our results. In this work, we focus on

*rostmar@okstate.edu
†cvasquez@usb.ve

describing NNMs of the beating response by analyzing the structure in the Fourier spectrum of the time series, where we have identified a closure of a multifrequency response that follows Eq. (8).

This report is divided into two fundamental parts: the calculation of the resonance curves (Secs. II and III) and the consequent study of the beating response related to NNMs (Sec. IV) analyzing the time series, Poincaré maps, phase space $(x_i, \dot{x}_i)$, and the configuration space (x_i, x_j) [1]. The last three tools are widely used in the study of trajectories of orbiting objects such as asteroids, planets, and spacecraft [32–34].

II. ANALYTICAL STUDY OF *N* LINEARLY COUPLED DUFFING OSCILLATORS

The Duffing equation follows the same structure as the harmonic oscillator adding a cubic term multiplied by a nonlinear coefficient γ, generally related to the system's stiffness [5]. By including an external sinusoidal driving force F at a fixed frequency Ω, a damping term ζ, and with a natural frequency of the underlying linear oscillator ω_0^2, the Duffing equation takes the form

$$\ddot{x} + \zeta\dot{x} + \omega_0^2 x + \gamma x^3 = F\cos\Omega t. \tag{1}$$

This system is generalized to N linearly coupled oscillators by including a linear coupling term δ, and by applying a driving force only to the first oscillator, resulting in the following system of equations

$$\begin{aligned}
&\ddot{x}_1 + \zeta\dot{x}_1 + \omega_0^2 x_1 + \gamma x_1^3 + \delta(x_1 - x_2) = F\cos\Omega t\\
&\ddot{x}_2 + \zeta\dot{x}_2 + \omega_0^2 x_2 + \gamma x_2^3 + \delta(x_2 - x_1)\\
&\quad + \delta(x_2 - x_3) = 0\\
&\vdots\\
&\ddot{x}_i + \zeta\dot{x}_i + \omega_0^2 x_i + \gamma x_i^3 + \delta(x_i - x_{i-1})\\
&\quad + \delta(x_i - x_{i+1}) = 0\\
&\vdots\\
&\ddot{x}_N + \zeta\dot{x}_N + \omega_0^2 x_N + \gamma x_N^3 + \delta(x_N - x_{N-1}) = 0
\end{aligned} \tag{2}$$

For two oscillators the set of equations reduces to

$$\begin{aligned}
&\ddot{x}_1 + \zeta\dot{x}_1 + \omega_0^2 x_1 + \gamma x_1^3 + \delta(x_1 - x_2) = F\cos\Omega t\\
&\ddot{x}_2 + \zeta\dot{x}_2 + \omega_0^2 x_2 + \gamma x_2^3 + \delta(x_2 - x_1) = 0.
\end{aligned} \tag{3}$$

Then, by applying perturbation theory at multiple timescales in the long-time stationary regime [5,28,35], we use a solution of the form $x_i(t) = A_i(t)\cos[\Omega t - \theta_i(t)]$, allowing to define the following dynamical system

$$\begin{aligned}
\dot{A}_1 &= -\frac{\zeta A_1}{2} + \frac{\delta A_2}{2\Omega}\sin(\theta_1 - \theta_2) + \frac{F}{2\Omega}\sin\theta_1\\
\dot{A}_2 &= -\frac{\zeta A_2}{2} - \frac{\delta A_1}{2\Omega}\sin(\theta_1 - \theta_2).
\end{aligned} \tag{4}$$

The solution of this system at fixed points gives its resonance curves. But it can also be solved numerically, allowing us to observe the system's behavior through phase portraits, Poincaré maps, configuration space projections, and time series with their corresponding Fourier transforms [1]. From Eq. (4) a relation between amplitudes A_i and the forcing frequency Ω is obtained with the use of the fixed-point equations ($\dot{A}_1 = \dot{A}_2 = 0$):

$$\begin{aligned}
A_1^2\left(\zeta^2\Omega^2 + u_1^2\right) + A_2^2(\delta^2 + 2\zeta^2\Omega^2) - 2A_2^2 u_1 u_2 &= F^2\\
A_2^2\left(u_2^2 + \zeta^2\Omega^2\right) - \delta^2 A_1^2 &= 0,
\end{aligned} \tag{5}$$

where $u_i \equiv \omega_0^2 - \Omega^2 + \delta + \frac{3}{4}\gamma A_i^2$ [29]. In the next section, an algebraic procedure to solve this system of equations is thoroughly described.

In an analogous way, the system of three, four, and five oscillators is solved, which gives the sets of Eqs. (B1), (B2), and (B3) respectively in Appendix B. These sets of equations follow a pattern that allows us to establish a recursion formula that serves as an analytical solution to N–coupled oscillators that relates the amplitudes of the oscillators with the forcing frequency as the following system of equations

$$\begin{aligned}
&\sum_{i=k+2}^{N} A_i^2[2\zeta^2\Omega^2 + (-1)^{i-k}2u_k u_i] - \delta^2 A_{k-1}^2 + A_k^2\left(\zeta^2\Omega^2 + u_k^2\right)\\
&\quad + A_{k+1}^2(\delta^2 + 2\zeta^2\Omega^2 - 2u_k u_{k+1}) = 0,
\end{aligned} \tag{6}$$

where $k = 1, \cdots, N$ is an index that corresponds to the number of the equation in the system, $A_0^2 = F^2/\delta^2$, and $A_i = 0$ when $i > N$.

Solving these equations is not an easy task, since they are in the form of a high-order polynomial, i.e., for a chain of two oscillators they result in a ninth-order polynomial, for three oscillators in a twenty-seventh order polynomial, etc. Therefore, numerical methods are needed to complement this analytical approach. For a chain of two oscillators, the set of Eqs. (5), could be solved with numerical methods such as the multivariate Newton-Raphson (NR) [36], or the eigenvalue decomposition method [37]. However, for more than two oscillators, the intrinsic instabilities of the method cause it to diverge. This limitation could be overcome by applying a suitable numerical method to find the root of high-order polynomials, but such a study is outside the scope of this report.

III. RESONANCE CURVES OF TWO LINEARLY COUPLED DUFFING OSCILLATORS

In this section, we study in detail the behavior of the resonance curves for a chain of two oscillators as a function of driving frequency, strength, stiffness, and damping. This has previously been studied [29] by applying the NR method to Eqs. (5). In that work, the authors considered the resonance curves for small/intermediate values of stiffness γ and driving force strength F, which are too small to observe large distortions in the second resonance peak. In contrast, here we focus on large values of γ and F, and discover large, previously missed distortions. Interestingly, such distorted unstable regions are related to a beating response associated with NNMs, as shown in the following section.

To solve Eqs. (5) for the oscillators' amplitudes A_i as a function of the other parameters, we first find A_1 as a function of A_2 from the second equation in Eqs. (5). Then, we substitute it in the first equation, which gives an explicit ninth-order polynomial in A_2. Details on this calculation and

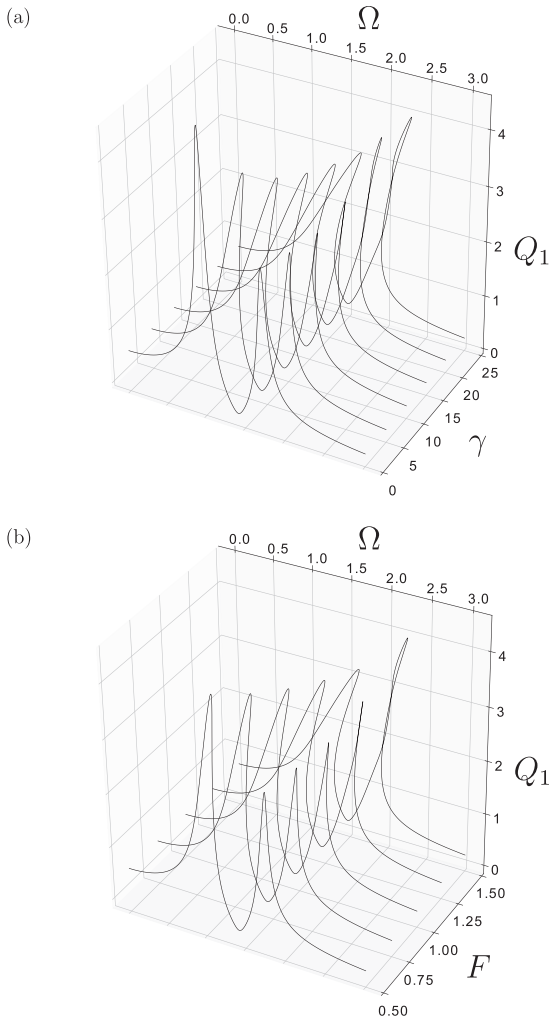

FIG. 1. Appearance of hysteresis. Resonance curves of the first oscillator with amplitude Q_1 and fixed parameters $\omega_0^2 = 1$, $\zeta = 0.1$, $\delta = 1$. (a) Varying γ and Ω at fixed $F = 0.1$. (b) Varying F and Ω at fixed $\gamma = 0.1$.

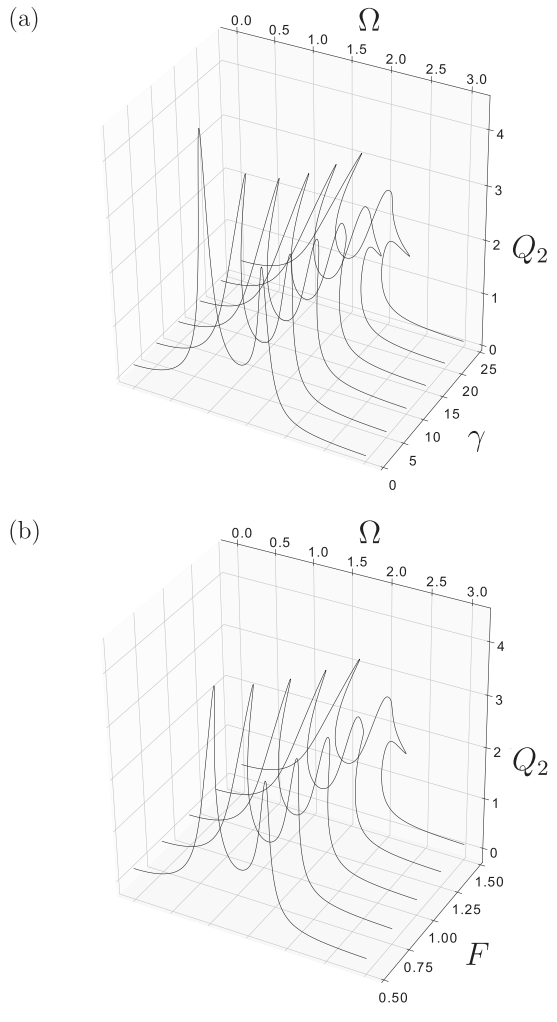

FIG. 2. Appearance of hysteresis. Resonance curves of the second oscillator with amplitude Q_2 and fixed parameters $\omega_0^2 = 1$, $\zeta = 0.1$, $\delta = 1$. (a) Varying γ and Ω at fixed $F = 0.1$. (b) Varying F and Ω at fixed $\gamma = 0.1$.

the polynomial coefficients are shown in Appendix A. This allows us to use the eigenvalue decomposition method to find the roots of this polynomial, i.e., A_2, and subsequently, obtain A_1 from the second equation. Then, we introduce scaled variables $Q_i \equiv A_i/F$.

Thus, having obtained the oscillators' scaled amplitudes as a function of system parameters, we now plot the resonance curves in Figs. 1 and 2, which show the amplitude of the corresponding oscillator Q_i as a function of the stiffness γ and driving frequency Ω at fixed driving force strength F in panel (a), and as a function of the driving force strength F and driving frequency Ω at fixed stiffness γ in panel (b). As γ and F increase [in panel (a) and (b), respectively] we observe the appearance of hysteresis in the resonance curves, i.e., regions with multiple solutions for Q_i. The presence of multivalued regions implies the existence of multiple root solutions to the polynomial equation that has to be properly taken into account in the chosen numerical method, as explained in Appendix C.

In Figs. 1 and 2 there are two peaks associated with resonances, as observed in the case of two coupled linear oscillators, but here with the characteristic hysteretic *bending* known to occur for the Duffing oscillator [5]. For low values of stiffness γ at fixed $F = 0.1$ these curves have previously been obtained in Ref. [29]. However, when F and γ increase, more complex structures than just the bending of the peaks appear. For large values of γ we observe in Q_1 a fold bifurcation [15], which indicates a stability change for the periodic solutions resulting from the system's hardening behavior [38]. Fold bifurcations are characteristic of nonlinear systems; in particular, they relate to NNMs and quasiperiodic solutions of the system [6,15,28,38]. In these hysteresis regions, there is the coexistence of stable and unstable points in the system, detailed in Fig. 9 of Appendix C.

We compare the resonance curves of this analytic approach with solving the differential Eqs. (3) numerically, where hysteresis also arises, as pictured in Fig. 10 of Appendix D. To solve this system numerically we implement a fourth-order vectorial Runge-Kutta method (RK4) [39]. As these numerical calculations also present hysteresis in some regions of the resonance peaks, we solve the differential equations by

both increasing and decreasing continuously Ω, which gives different results in the hysteretic region of the resonance peaks due to their sensitivity to the initial conditions.

In general, the theoretical and numerical resonance curves show good agreement. Still, in multivalued regions some amplitude values cannot be obtained by the chosen numerical approach, demonstrating the benefit of using the recursion relation along with the eigenvalue decomposition method. These hysteretic regions are of great interest, especially around the second resonance peak, where the system exhibits a quasiperiodic beating-oscillation response to perturbations which we analyze next.

IV. BEATING OSCILLATIONS AND NONLINEAR NORMAL MODES IN A CHAIN OF TWO OSCILLATORS

Next, we study the response of the system to amplitude perturbations in the unstable region around the second resonance peak. We find a stationary quasiperiodic beating oscillation in the time series of the oscillator coordinates. We analyze these patterns in the time domain, and in terms of their Fourier spectrum.

We demonstrate that they correspond to NNMs in the following definition [24]: For a general mechanical system described by $x = (q, \dot{q})$, and the equations of motion

$$\dot{x} = Ax + f_0(x) + \epsilon f_1(x, \Omega t; \epsilon),$$
$$f_0(x) = O(|x^2|); \quad 0 \leqslant \epsilon \ll 1, \tag{7}$$

a NNM is defined as the closure of a multifrequency solution

$$x(t) = \sum_{|m|=1}^{\infty} x_m e^{i\langle m, \Omega\rangle t}, \quad m \in \mathbb{N}^f, \quad \Omega \in \mathbb{R}^f \tag{8}$$

of the nonlinear system in Eq. (7), where $f \in \mathbb{N}$ is the number of frequencies, the vector m is a multi-index of non-negative integers, and $x_m \in \mathbb{C}^n$ are the complex Fourier amplitudes of the real solution $x(t)$ with respect to frequencies in the frequency vector $\Omega = (\Omega_1, \ldots, \Omega_f)$.

In addition, we inspect the correspondent phase-space and Poincaré maps, which are suitable techniques to characterize quasiperiodic oscillations [40].

A. Time series and Fourier spectra

For large values of stiffness γ at characteristic driving frequencies Ω in the unstable region of the second resonance peak, the system oscillates showing quasiperiodic beating responses in the position-time series that are sensitive to the initial conditions. This sensitivity is particularly pronounced for initial conditions with amplitudes slightly larger than the resonance curve's amplitudes. Figure 3 shows the position (x_i) time series of both oscillators and the corresponding Fourier spectrum for different large values of γ. This quasiperiodic beating is associated with NNMs and it is similar to what has been already characterized for a linear cantilever beam attached to ground through a strongly nonlinear stiffness at its free boundary [17]. We confirm the presence of NNMs by calculating the Fourier transform of the time series, which shows clusters of frequencies that are described by Eq. (8). This means that these clusters are related to a closure of a

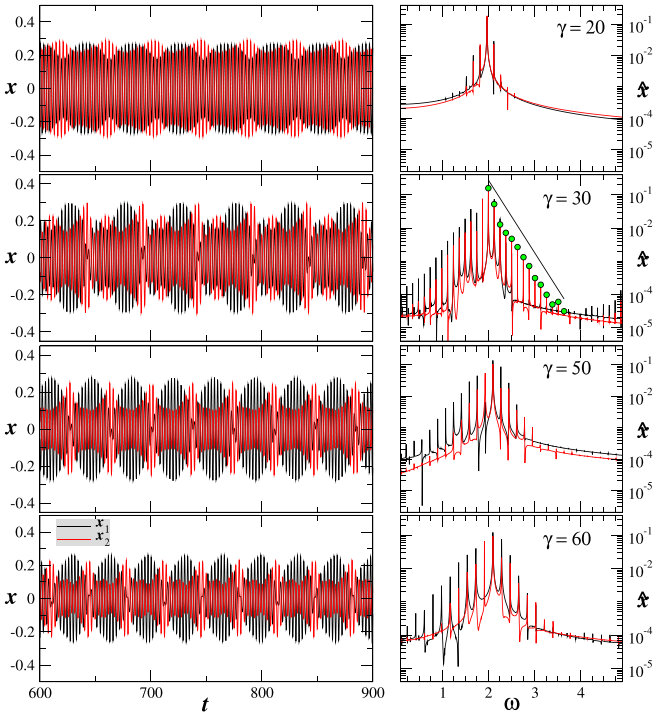

FIG. 3. Beat response in the system's time series, and clusters of frequencies in Fourier space. Time series (left) and Fourier transform (right). Parameters: $\omega_0^2 = 1$, $\zeta = 0.1$, $\delta = 1$, $F = 0.1$; initial conditions: $x_{1,2}(0) = 0.3$, $\dot{x}_{1,2}(0) = 0$. Frequencies: $\Omega = 1.97$ ($\gamma = 20$), $\Omega = 2$ ($\gamma = 30$), $\Omega = 2.1$ ($\gamma = 50, 60$) from top to bottom row. The line *lin-log* (see text) has been scaled by a 2 factor to emphasize the correspondence between slopes.

multifrequency solution of the system, following the already stated definition of NNMs [24]. Figure 3 focuses on only one cluster of frequencies, but the Fourier spectrum can have more than one cluster of frequencies which amplitudes decrease by an order of magnitude or more from cluster to cluster when ω increases, as portrayed in Fig. 4. Although secondary clusters have a significantly smaller amplitude, they still contribute to the time series, thus, these beating responses are associated with a single NNM or a combination of several NNMs.

Now, we consider in greater detail a specific characteristic value of stiffness γ, i.e., $\gamma = 30$, which is above the transition from stable resonance to unstable hysteretic resonance, shown in the second row of Fig. 3. The right panel shows a cluster of Fourier amplitude peaks that decay exponentially from a central peak, highlighted with green points. Performing an exponential fit to these points gives the *lin-log* line shown in Fig. 3, which has the form

$$\hat{x}_{\max} \sim \exp[-\ln(8)(\omega_{\max} - \Omega)],$$

where $\omega_{\max} - \Omega \simeq 0.0125\,k$, $k = 0, 1, \cdots, 12$ ($R^2 \approx 0.99$).

This exponential decay of the Fourier components suggests the following (approximate) expression for the time series as an expansion around the main maximum ($k = 0$)

$$\begin{aligned} x = {} & a^{-\mathcal{N}} e^{i(\Omega - \mathcal{N}\nu)t} + \cdots + a^{-2} e^{i(\Omega - 2\nu)t} \\ & + a^{-1} e^{i(\Omega - \nu)t} + e^{i\Omega t} + a^{-1} e^{i(\Omega + \nu)t} \\ & + a^{-2} e^{i(\Omega + 2\nu)t} + \cdots + a^{-N} e^{i(\Omega + \mathcal{N}\nu)t}, \end{aligned} \tag{9}$$

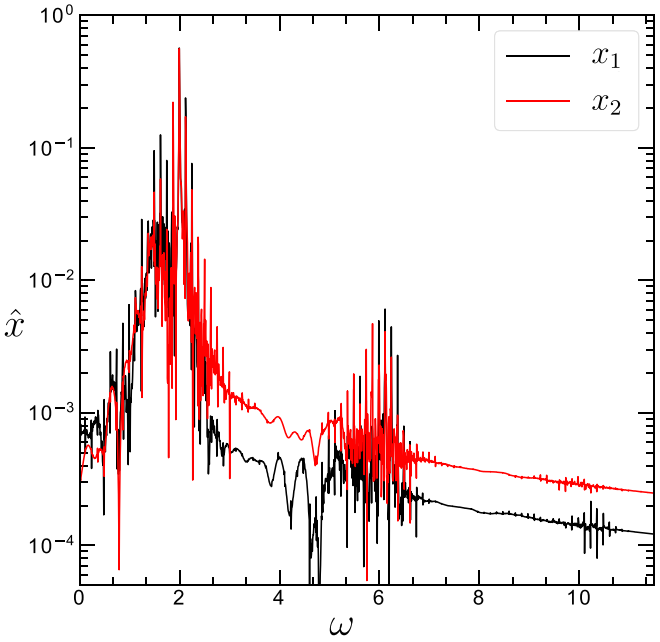

FIG. 4. Multiple clusters of frequencies in Fourier space. Detailed Fourier spectrum of time series shown for $\gamma = 30$ over a wider range of frequencies ω (c.f. Fig. 3). A main cluster of frequencies is identified for $\omega \sim 2$, and two secondary clusters as ω increases around $\omega \sim 6$ and $\omega \sim 10$. The amplitude of each cluster reduces about an order of magnitude as ω increases from cluster to cluster.

where $\mathcal{N}$ is the number of subsequent peaks from one side of the central maximum in the cluster.

Thus, the oscillations of the system can be written as

$$x = \mathcal{R}e[e^{i\Omega t}(a^{-\mathcal{N}}e^{-\mathcal{N}i\nu t} + \cdots + a^{-2}e^{-2i\nu t} + a^{-1}e^{-i\nu t} + 1 + a^{-1}e^{i\nu t} + a^{-2}e^{2\nu t} + \cdots + a^{\mathcal{N}}e^{-\mathcal{N}i\nu t})], \quad (10)$$

$$x = \cos(\Omega t)\left[1 + 2\sum_{k=1}^{\mathcal{N}} a^{-k}\cos(k\nu t)\right]. \quad (11)$$

The series in Eq. (11) is an approximation of the numerical complex-beat result taking into account just the first cluster of frequencies, e.g., the clusters in the Fourier spectrum shown in Fig. 3. This expression reproduces the beating responses seen in the full time series arising from clusters of frequencies as we demonstrate in Fig. 5. There, we compare two different

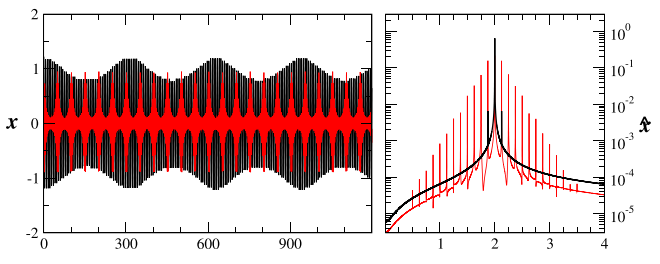

FIG. 5. Approximation of beating NNMs. Theoretical time series (left) and Fourier transform (right) obtained from Eq. (11). Parameters: $\mathcal{N} = 2$, $\nu = 0.02$, $a = 10$ in black and $\mathcal{N} = 12$, $\nu = 0.0125$, $a = 8$ in red.

values of $\mathcal{N}$. When $\mathcal{N} = 12$ (in red) the Fourier spectrum has a cluster of twenty-five frequency peaks, and by following Eq. (8) the system has dimension $f = 12$. Similarly, when $\mathcal{N} = 2$ (in black) the system has a smaller cluster with three peaks with dimension $f = 3$. The time series of these two examples show how the envelope of the beat increases in frequency as $\mathcal{N}$ increases.

B. Phase space and Poincaré maps

Here we explore the characteristics of the system that emerge from the study of its Poincaré maps, phase space $(x_i, \dot{x}_i)$, and the configuration space (x_i, x_j) when it is beating with NNMs.

The two-dimensional (2D) phase space is one good example of them, which is commonly used to describe the states of the system. When $\gamma = 30$ we can predict that the first oscillator in our chain will behave similarly to a single forced and damped Duffing oscillator by looking at their 2D phase space, which both show a similar limit cycle [5], portrayed in Fig. 11 of Appendix E. However, we obtain more information about the system by looking at three-dimensional (3D) projections of the phase space. Figure 6 shows two 3D projections of the phase space using the same parameters as in Fig. 3 when $\gamma = 30$ for both oscillators, shown in panels (a) and (b). Both panels present a similar behavior, they show a folded tori, which is characteristic of quasiperiodic trajectories. When a system presents quasiperiodic oscillations, its characteristic frequencies are incommensurate to each other, causing the phase trajectory to return close but never to the exact same point, thus, evolving along the surface of an invariant torus [30]. Specifically, these tori families are associated with quasi-halo and Lissajous orbits [33,34]. The unaligned lines arise from the transient response of the system. Poincaré maps are a useful tool when dealing with long or high-dimensional phase space trajectories, i.e., they focus on the behavior of the system at specific moments in time without needing to track the full trajectory of the system [1]. Figure 7 displays the Poincaré section of the time series in Fig. 3 for $\gamma = 30$, it shows a curve that self-intersects, which represents the folding of the tori previously shown in Fig. 6. We also note that the sections in Fig. 7 resemble the attractors obtained in a chain of two damped and forced Duffing oscillators with different potentials [26]. This is another feature of quasiperiodic orbits, which are usually represented by single or multiple closed curves [30] that represent cross-sections of the toroidal attractors [33,41]. The sparse points represent the transient response of the system.

Another way to observe the system's behavior is through 2D and 3D projections of the configuration space, where the trajectories of each oscillator are compared. Configuration spaces are popular for predicting the orbits of space objects [32] because they map the position of each object to another. Figure 8 shows a 2D projection of the configuration space of both oscillators. The black lines correspond to the vertical projection of any of the tori in Fig. 6, while the different strips correspond to representative Poincaré sections of the positions with different initial points t_0. This configuration space follows the same parameters as in Fig. 6. It shows how the amplitude of the oscillators relate to each other, and it

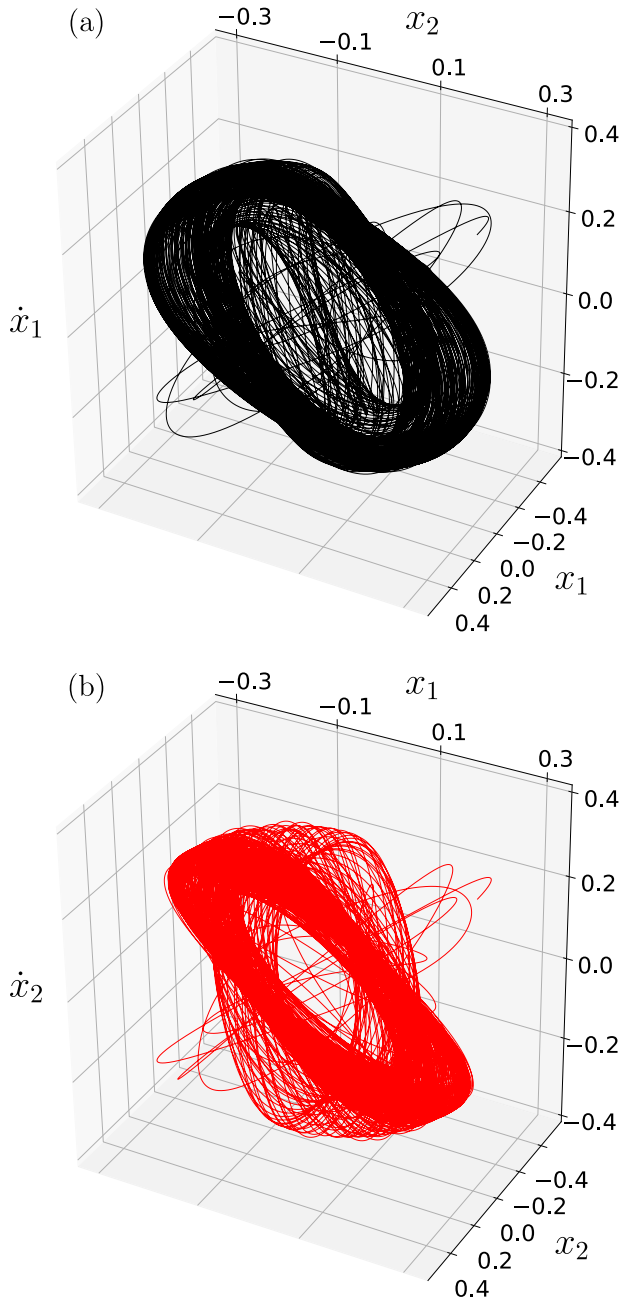

FIG. 6. Quasiperiodic trajectories folded tori. 3D projections of the phase-space coordinates for the same parameters as the time series shown in Fig. 3 for $\gamma = 30$, (a) including the velocity of the first oscillator ($\dot{x}_1$), and (b) including the velocity of the second oscillator ($\dot{x}_2$).

is just another way to display the system's dynamics. For example, a vertical line at $x_1 = 0$ will show all the possible amplitudes of the second oscillator when the first one is at the position of equilibrium. Another analogous example happens for a horizontal line at $x_2 = 0$.

V. CONCLUSIONS

In this work we considered a paradigmatic nonlinear dynamical system in the form of a chain of N linearly coupled damped Duffing oscillators with a periodic driving force acting on the first oscillator, using two complementary approaches, e.g., time-series analysis and phase-space portraits.

Using an analytical approach we found algebraic equations that give a general solution of the N oscillator chain, which allow us to obtain the resonance curves of the system.

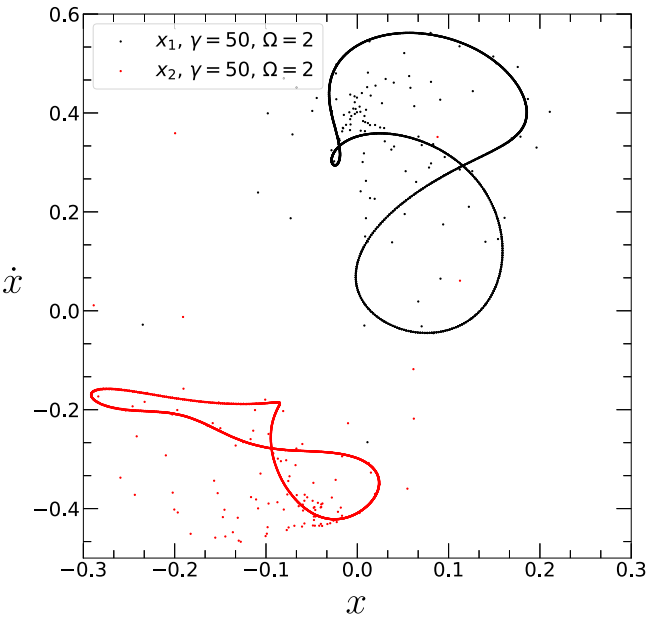

FIG. 7. Poincaré section displaying closed curves. Poincaré map corresponding to results in Fig. 3 for $\gamma = 30$. These self-intersecting patterns represent the folding of the tori in phase space.

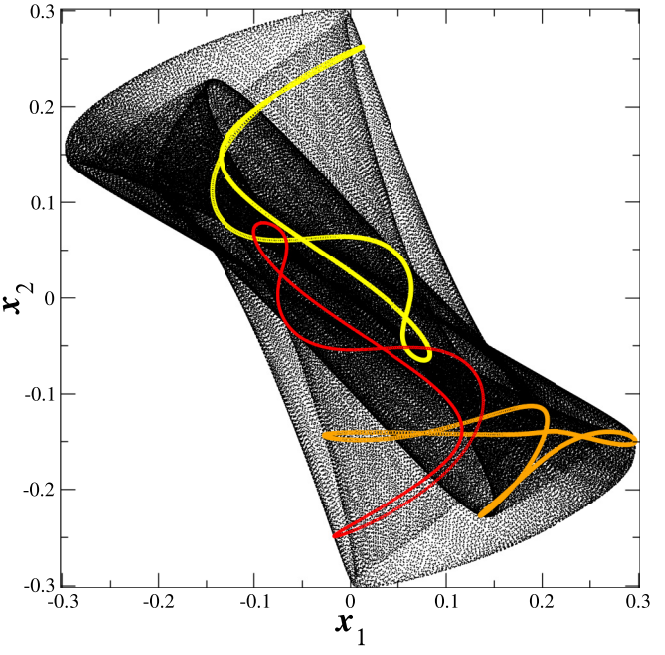

FIG. 8. Configuration space, 2D projection of any of the folded tori in Fig. 6. The strips correspond to Poincaré sections for the same variables taken with different initial points.

However, this approach presents a numerical challenge that still needs to be solved, as it requires obtaining the roots of polynomials of an order that rapidly increases with the number of oscillators N.

We then studied in detail the case of two oscillators for large values of stiffness γ and driving force amplitude F. We first analyzed the resulting resonance curves: As γ or F increased, the resonance curves showed large deformations on the second resonance peak and a bending (Duffing-type) on the first resonance peak. Both peaks presented hysteresis when approached with numerical methods.

While studying these resonance curves, specifically the unstable region close to the second resonant peak, the system presented nonlinear beating responses in the stationary regime for different large values of γ. Our analysis demonstrates the presence of NNMs by inspecting the Fourier spectrum of the nonlinear beating responses in the time series, where we identified clusters of frequencies that relate directly with quasiperiodic NNMs [24]. We characterized these clusters and chose one as a sample ($\gamma = 30$) to apply the NNMs definition and successfully reproduced a beating response.

Besides inspecting the system's time series, quasiperiodic oscillations can be described by the system's phase space and Poincaré map. We calculated the phase space of the beating response, which showed folded toroidal structures which are characteristic of quasiperiodic oscillations. Also, we inspected the Poincaré maps which showed closed curves that are another characteristic of quasiperiodic oscillations and represent cross-sections of the folded tori. We conclude that by increasing the nonlinearity of the system, i.e., for large stiffness (γ) values, this system can produce beating quasiperiodic oscillations, which are characteristic of NNMs. Nonbeating responses in phase space will just have plane-limit cycles (periodic oscillations), but not nonplanar structures. This shows that beating oscillations related to NNMs can also be described by their quasiperiodicity through traditional techniques such as by inspecting the phase space and Poincaré maps.

Remarkably, all these complex features of the dynamics already appear for just two coupled oscillators, demonstrating the richness of nonlinear coupled systems. Our work points to some open questions for future investigation: Do the observed beating response and NNMs relate to the number of oscillators in the chain? And if they are related, how does the number of oscillators affect the response of the system in the unstable region of their resonance curves? Once this relation has been established, the problem of several discrete coupled Duffing oscillators and their approximation to a continuum would be an interesting problem to explore that might help model one-dimensional stiff systems like a cable or a bar.

ACKNOWLEDGMENTS

We thank Dr. Thomas Bilitewski, professor at Oklahoma State University, very much for the comments that greatly improved the manuscript and his guidance in the submission process. We are also grateful to Dr. Mario F. Borunda, professor at Oklahoma State University, for his mentorship and support during the development of this manuscript.

APPENDIX A: AMPLITUDE CALCULATION FOR TWO OSCILLATORS

Using the second equation in Eqs. (5) of the main manuscript, we establish a relation between the amplitudes of both oscillators:

$$A_1 = A_2 \frac{u_2^2 + \zeta^2 \Omega^2}{\delta^2}. \tag{A1}$$

By substituting this expression in the first equation of Eqs. (5), and recalling that $u_i \equiv \omega_0^2 - \Omega^2 + \delta + \frac{3}{4}\gamma A_i^2$, we find a polynomial equation of the form

$$\sum_{i=0}^{9} p_i A_2^i = 0, \tag{A2}$$

with the following coefficients p_i:

$$\begin{aligned}
p_9 &= b_1 a_1^2, \\
p_8 &= 2b_1 a_1 a_2 + b_2 a_1^2, \\
p_7 &= b_1\left(2a_1 a_3 + a_2^2\right) + 2b_2 a_1 a_2 + b_3 a_1^2, \\
p_6 &= b_1(2a_1 a_0 + 2a_2 a_3) + b_2\left(2a_1 a_3 + a_2^2\right) + 2b_3 a_1 a_2, \\
p_5 &= b_1\left(2a_2 a_0 + a_3^2\right) + b_2(2a_1 a_0 + 2a_2 a_3) \\
&\quad + b_3\left(2a_1 a_3 + a_2^2\right) - \tfrac{3}{2}\gamma a_1, \\
p_4 &= 2b_1 a_3 a_0 + b_2\left(2a_2 a_0 + a_3^2\right) \\
&\quad + b_3(2a_1 a_0 + 2a_2 a_3) - \tfrac{3}{2}\gamma a_2 - 2a_0 a_1, \\
p_3 &= b_1\left(a_0^2 + \zeta^2(\Omega^2) + 2b_2 a_3 a_0\right. \\
&\quad + b_3\left(2a_2 a_0 + a_3^2\right) - \tfrac{3}{2}\gamma a_3 - 2a_0 a_2, \\
p_2 &= b_2\left(a_0^2 + \zeta^2\Omega^2\right) + 2b_3 a_3 a_0 - \tfrac{3}{2}\gamma a_0 - 2a_0 a_3, \\
p_1 &= b_3\left(a_0^2 + \zeta^2\Omega^2\right) + 2\zeta^2\Omega^2 + \delta^2 - 2a_0^2, \\
p_0 &= -F^2,
\end{aligned}$$

where the supporting constants a_i and b_i are

$$\begin{aligned}
a_0 &= \omega_0^2 - \Omega^2 + \delta, \\
a_1 &= \frac{27\gamma^3}{64\delta^2}, \\
a_2 &= \frac{9\gamma^2 a_0}{8\delta^2}, \\
a_3 &= \frac{3\gamma a_0^2 + 3\gamma\zeta^2\Omega^2}{4\delta^2}, \\
b_1 &= \frac{9\gamma^2}{16\delta^2}, \\
b_2 &= \frac{3\gamma a_0}{2\delta^2}, \\
b_3 &= \frac{\zeta^2\Omega^2 + a_0^2}{\delta^2}.
\end{aligned}$$

APPENDIX B: AMPLITUDE-FREQUENCY SYSTEM OF EQUATIONS FOR THREE, FOUR, AND FIVE OSCILLATORS

Analogously as we obtained the system of Eqs. (5) in the main manuscript, we apply the perturbation theory at multiple timescales in the long-time stationary regime to obtain fixed points of the dynamical system that results in the system of Eqs. (B1), (B2), and (B3) which relate amplitudes and forcing frequencies for chains of three, four, and five oscillators respectively.

$$
\begin{aligned}
&-F^2+A_1^2\left(\zeta^2\Omega^2+u_1^2\right)+A_2^2(\delta^2+2\zeta^2\Omega^2-2u_2u_1)\\
&\quad+A_3^2(2\zeta^2\Omega^2+2u_3u_1)=0\\
&\quad-\delta^2A_1^2+A_2^2\left(\zeta^2\Omega^2+u_2^2\right)+A_3^2(2\zeta^2\Omega^2-2u_3u_2+\delta^2)=0\\
&\quad A_3^2\left(\zeta^2\Omega^2+u_3^2\right)-\delta^2A_2^2=0. \qquad \text{(B1)}\\
&-F^2+A_1^2\left(\zeta^2\Omega^2+u_1^2\right)+A_2^2(\delta^2+2\zeta^2\Omega^2-2u_1u_2)\\
&\quad+A_3^2(2\zeta^2\Omega^2+2u_1u_3)+A_4^2(2\zeta^2\Omega^2+2u_1u_4)=0\\
&-\delta^2A_1^2+A_2^2\left(\zeta^2\Omega^2+u_2^2\right)+A_3^2(\delta^2+2\zeta^2\Omega^2-2u_2u_3)\\
&\quad+A_4^2(2\zeta^2\Omega^2+2u_2u_4)=0\\
&-\delta^2A_2^2+A_3^2\left(\zeta^2\Omega^2+u_3^2\right)+A_4^2(\delta^2+2\zeta^2\Omega^2-2u_3u_4)=0\\
&\quad-\delta^2A_3^2+A_4^2\left(d^2\Omega^2+u_4^2\right)=0. \qquad \text{(B2)}\\
&-F^2+A_1^2\left(\zeta^2\Omega^2+u_1^2\right)+A_2^2(\delta^2+2\zeta^2\Omega^2-2u_1u_2)\\
&\quad+A_3^2(2\zeta^2\Omega^2+2u_1u_3)+A_4^2(2\zeta^2\Omega^2+2u_1u_4)\\
&\quad+A_5^2(2\zeta^2\Omega^2+2u_1u_5)=0\\
&-\delta^2A_1^2+A_2^2\left(\zeta^2\Omega^2+u_2^2\right)+A_3^2(\delta^2+2\zeta^2\Omega^2-2u_2u_3)\\
&\quad+A_4^2(2\zeta^2\Omega^2+2u_2u_4)+A_5^2(2\zeta^2\Omega^2-2u_2u_5)=0\\
&-\delta^2A_2^2+A_3^2\left(\zeta^2\Omega^2+u_3^2\right)+A_4^2(\delta^2+2\zeta^2\Omega^2-2u_3u_4)\\
&\quad+A_5^2(2\zeta^2\Omega^2+2u_1u_5)=0\\
&-\delta^2A_3^2+A_4^2\left(\zeta^2\Omega^2+u_4^2\right)+A_5^2(\delta^2+2\zeta^2\Omega^2-2u_4u_5)=0\\
&\quad-\delta^2A_4^2+A_5^2\left(\zeta^2\Omega^2+u_5^2\right)=0. \qquad \text{(B3)}
\end{aligned}
$$

As we increase N from 2 to 5, these sets of equations follow a pattern that allows us to establish a general recursion formula capable of reproducing all of these sets of equations. This formula is presented in Eq. (6) and discussed in the main work.

APPENDIX C: STABILITY IN THE RESONANCE CURVES

The stability in the hysteretical regions is an interesting characteristic of the system. By solving the Eqs. (5) using the eigenvalue decomposition method we find all the root solutions of the polynomial. Then, we identify stable and unstable regions by studying the system's eigenvalues in each region [1]. The solid lines in Fig. 9 represent the solution of the polynomial using the eigenvalue decomposition method; the black lines show the stable roots while the red lines show the unstable roots.

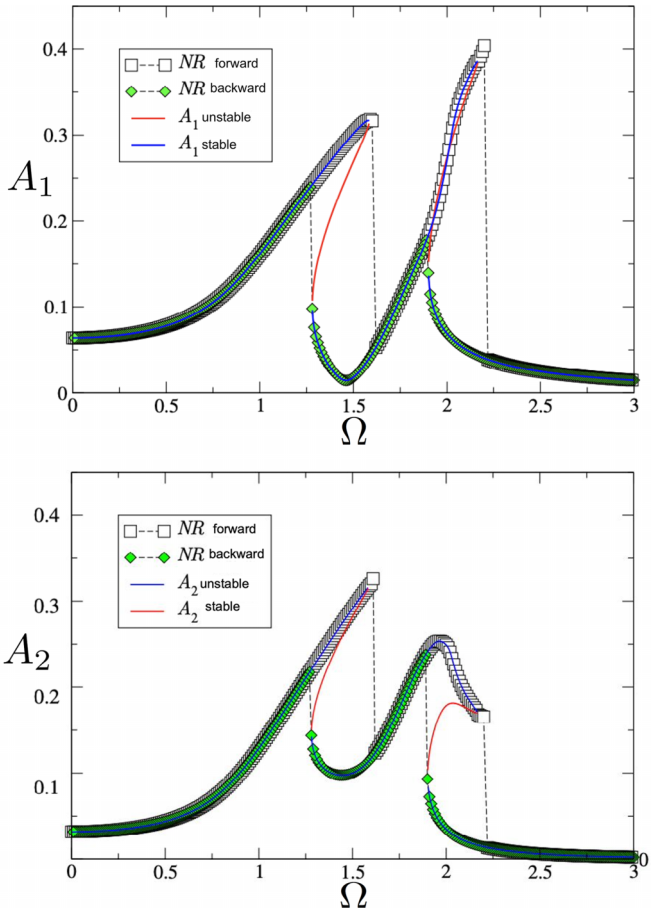

FIG. 9. Theoretical resonance curves for both oscillators' amplitudes (A_i), comparing the NR (markers) and eigenvalue decomposition (solid line) methods. The first oscillator is on top. Parameters used: $\omega_0^2=1$, $\zeta=0.1$, $\delta=1$, $\gamma=20$ and $F=0.1$. The forward and backward labels refer to applying the NR method increasing and decreasing Ω respectively.

The limitation of some numerical methods such as the NR method arises in unstable regions. For example, in Fig. 9 we employ the NR method either by increasing (forward, white square markers) or decreasing (backward, green diamond markers) the driving frequency Ω. We notice jumps up or down at different curve points, but the NR method always avoids unstable branches following the closest stable amplitude accordingly.

APPENDIX D: COMPARISON BETWEEN ANALYTICAL AND NUMERICAL RESONANCE CURVES

Here we contrast the numerical and theoretical resonance curves for $N=2$ oscillators, obtaining Fig. 10. The theoretical results follow Eqs. (5) as explained in Sec. III of the main work. We employ a fourth-order vectorial Runge-Kutta method (RK4) for the numerical results. Since this differential equation solver method only gives one result at a time, we decided to apply it while increasing and decreasing the value of Ω to confirm the presence of hysteresis. Although the numerical results do not explore all the unstable regions that

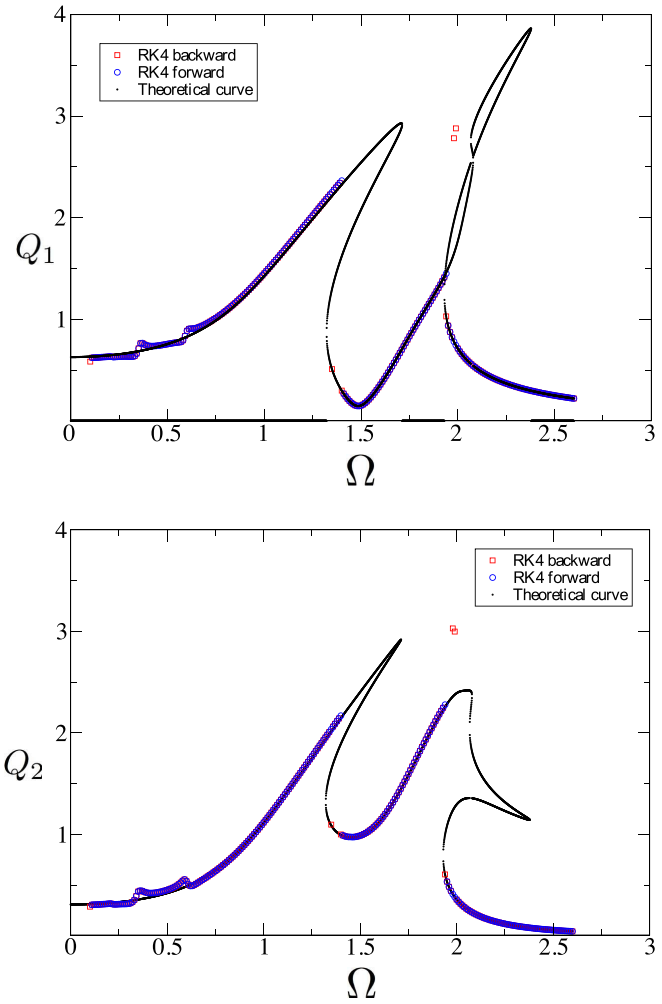

FIG. 10. Comparison between the numerical and theoretical resonance curves for both oscillators' scaled amplitudes Q_i. The first oscillator is on top. Parameters used: $\omega_0^2 = 1$, $\zeta = 0.1$, $\delta = 1$, $\gamma = 30$ and $F = 0.1$. The forward and backward labels refer to applying the RK4 method increasing and decreasing Ω respectively.

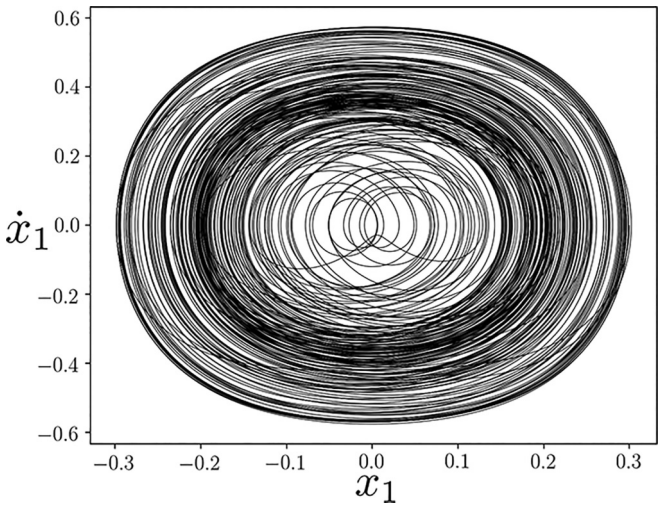

FIG. 11. Phase space $(x_1, \dot{x}_1)$ of the first oscillator related to Fig. 3 in the main manuscript for $\gamma = 30$.

the theoretical approach predicts, they still present hysteresis (red vs blue markers).

APPENDIX E: 2D PHASE–SPACE OF A CHAIN OF TWO OSCILLATORS

Phase-space portraits are another classic tool to represent the behavior of dynamical systems, allowing us to observe equilibrium points, limit cycles, chaos, etc. Figure 11 is an example of a phase portrait of the first oscillator in a chain of $N = 2$ oscillators at large stiffness values ($\gamma = 30$). We observe curves that, unlike periodic orbits, do not repeat exactly over time, indicating the repetitive nature of the quasiperiodic oscillations of the system. This also tells that the system has multiple characteristic frequencies (as shown in Figs. 3 and 4) but does not form a simple repeating pattern. This limit cycle resembles the patterns obtained for a single Duffing oscillator [5]. Also, the trajectories in Fig. 11 represent a side projection of the folded tori displayed in Fig. 6(a).

[1] S. Strogatz, *Nonlinear Dynamics and Chaos: With Applications to Physics, Biology, Chemistry, and Engineering* (CRC Press, 2018).

[2] D. Kaplan and L. Glass, *Understanding Nonlinear Dynamics*, Textbooks in Mathematical Sciences (Springer, New York, 1997).

[3] J. Thompson and H. Stewart, *Nonlinear Dynamics and Chaos*, Nonlinear Dynamics and Chaos (Wiley, 2002).

[4] G. Duffing, *Erzwungene Schwingungen Bei Veränderlicher Eigenfrequenz Und Ihre Technische Bedeutung*, Sammlung Vieweg (Vieweg, 1918).

[5] I. Kovacic and M. Brennan, *The Duffing Equation: Nonlinear Oscillators and their Behaviour* (Wiley, 2011).

[6] V. R. Tuz, B. A. Kochetov, L. A. Kochetova, P. L. Mladyonov, and S. L. Prosvirnin, Two-oscillator model of trapped-modes interaction in a nonlinear bilayer fish-scale metamaterial, Phys. Scr. **90**, 025504 (2015).

[7] J. M. Manimala and C. T. Sun, Numerical investigation of amplitude-dependent dynamic response in acoustic metamaterials with nonlinear oscillators, J. Acoust. Soc. Am. **139**, 3365 (2016).

[8] J. Fajans, E. Gilson, and L. Friedland, The effect of damping on autoresonant (nonstationary) excitation, Phys. Plasmas **8**, 423 (2001).

[9] D. Laxalde and F. Thouverez, Complex non-linear modal analysis for mechanical systems: Application to turbomachinery bladings with friction interfaces, J. Sound Vib. **322**, 1009 (2009).

[10] G. Donoso and C. L. Ladera, Nonlinear dynamics of a magnetically driven Duffing-type spring-magnet oscillator in the static magnetic field of a coil, Eur. J. Phys. **33**, 1473 (2012).

[11] S. I. Arroyo and D. H. Zanette, Duffing revisited: Phase-shift control and internal resonance in self-sustained oscillations, Eur. Phys. J. B **89**, 12 (2016).

[12] L. I. Manevitch, A. Kovaleva, V. Smirnov, and Y. Starosvetsky, *Nonstationary Resonant Dynamics of Oscillatory Chains and Nanostructures*, Foundations of Engineering Mechanics (Springer, Singapore, 2018).

[13] Y. Jia, Review of nonlinear vibration energy harvesting: Duffing, bistability, parametric, stochastic and others, J. Intell. Mater Syst. Struct. **31**, 921 (2020).

[14] Q. Wang, Y. Yang, and X. Zhang, Weak signal detection based on Mathieu-Duffing oscillator with time-delay feedback and multiplicative noise, Chaos Solit. Fractals **137**, 109832 (2020).

[15] R. Kuether, L. Renson, T. Detroux, C. Grappasonni, G. Kerschen, and M. Allen, Nonlinear normal modes, modal interactions and isolated resonance curves, J. Sound Vib. **351**, 299 (2015).

[16] F. Hocke, M. Pernpeintner, X. Zhou, A. Schliesser, T. J. Kippenberg, H. Huebl, and R. Gross, Determination of effective mechanical properties of a double-layer beam by means of a nano-electromechanical transducer, Appl. Phys. Lett. **105**, 133102 (2014).

[17] M. Kurt, M. Eriten, D. M. McFarland, L. A. Bergman, and A. F. Vakakis, Strongly nonlinear beats in the dynamics of an elastic system with a strong local stiffness nonlinearity: Analysis and identification, J. Sound Vib. **333**, 2054 (2014).

[18] M. G. Clerc, S. Coulibaly, M. A. Ferré, and R. G. Rojas, Chimera states in a Duffing oscillators chain coupled to nearest neighbors, Chaos **28**, 083126 (2018).

[19] M. Clerc, S. Coulibaly, and M. Ferré, Freak chimera states in a locally coupled duffing oscillators chain, Commun. Nonlinear Sci. Numer. Simul. **89**, 105288 (2020).

[20] G. Kerschen, J. Golinval, A. F. Vakakis, and L. A. Bergman, The method of proper orthogonal decomposition for dynamical characterization and order reduction of mechanical systems: an overview, Nonlinear Dyn. **41**, 147 (2005).

[21] G. Kerschen, K. Worden, A. F. Vakakis, and J. Golinval, Past, present and future of nonlinear system identification in structural dynamics, Mech. Syst. Signal Process. **20**, 505 (2006).

[22] G. Kerschen, M. Peeters, J. Golinval, and A. Vakakis, Nonlinear normal modes, part i: A useful framework for the structural dynamicist, Mech. Syst. Signal Process. **23**, 170 (2009), special Issue: Non-linear Structural Dynamics.

[23] A. Albu-Schäffer and C. Della Santina, A review on nonlinear modes in conservative mechanical systems, Annu. Rev. Control **50**, 49 (2020).

[24] G. Haller and S. Ponsioen, Nonlinear normal modes and spectral submanifolds: existence, uniqueness and use in model reduction, Nonlinear Dyn. **86**, 1493 (2016).

[25] L. Renson, G. Kerschen, and B. Cochelin, Numerical computation of nonlinear normal modes in mechanical engineering, J. Sound Vib. **364**, 177 (2016).

[26] U. E. Vincent and A. Kenfack, Synchronization and bifurcation structures in coupled periodically forced non-identical duffing oscillators, Phys. Scr. **77**, 045005 (2008).

[27] S. Belbasi, M. E. Foulaadvand, and Y. S. Joe, Anti-resonance in a one-dimensional chain of driven coupled oscillators, Am. J. Phys. **82**, 32 (2014).

[28] J. Warminski, Nonlinear normal modes of a self-excited system driven by parametric and external excitations, Nonlinear Dyn. **61**, 677 (2010).

[29] R. Jothimurugan, K. Thamilmaran, S. Rajasekar, and M. Sanjuán, Multiple resonance and anti-resonance in coupled duffing oscillators, Nonlinear Dyn. **83**, 1803 (2016).

[30] L. Kabiraj, A. Saurabh, P. Wahi, and R. Sujith, Experimental study of thermoacoustic instability in ducted premixed flames: periodic, quasi-periodic and chaotic oscillations, in *Proceedings of the n3I-Int'l Summer School and Workshop on Non-Normal and Nonlinear Effects in Aero- and Thermoacoustics, Munich, Germany* (2010), p. 12.

[31] L. Borkowski and A. Stefanski, Stability of the 3-torus solution in a ring of coupled duffing oscillators, Eur. Phys. J. Spec. Top. **229**, 2249 (2020).

[32] Y. Yu and H. Baoyin, Orbital dynamics in the vicinity of asteroid 216 kleopatra, Astronomical J. **143**, 62 (2012).

[33] E. Kolemen, N. J. Kasdin, and P. Gurfil, Quasi-periodic orbits of the restricted three-body problem made easy, AIP Conf. Proc. **886**, 68 (2007).

[34] A. Haapala and K. Howell, Trajectory design strategies applied to temporary comet capture including Poincaré maps and invariant manifolds, Celest. Mech. Dyn. Astron. **116**, 299 (2013).

[35] A. Nayfeh and D. Mook, *Nonlinear Oscillations*, Wiley Classics Library (Wiley, 2008).

[36] T. J. Ypma, Historical development of the Newton-Raphson method, SIAM Rev. Soc. Ind. Appl. Math. **37**, 531 (1995).

[37] R. A. Horn and C. R. Johnson, *Matrix Analysis* (Cambridge University Press, 2012).

[38] T. Detroux, L. Renson, L. Masset, and G. Kerschen, The harmonic balance method for bifurcation analysis of nonlinear mechanical systems, in *Nonlinear Dynamics, Volume 1: Conference Proceedings of the Society for Experimental Mechanics Series*, edited by G. Kerschen (Springer, 2016), pp. 65–82.

[39] L. Zheng and X. Zhang, Numerical methods, in *Modeling and Analysis of Modern Fluid Problems*, Mathematics in Science and Engineering (Academic Press, 2017), Chap. 8, pp. 361–455.

[40] C. Kaas-Petersen, Computation of quasi-periodic solutions of forced dissipative systems, J. Comput. Phys. **58**, 395 (1985).

[41] R. Vitolo, H. Broer, and C. Simo, Quasi-periodic bifurcations of invariant circles in low-dimensional dissipative dynamical systems, Regul. Chaotic Dyn. **16**, 154 (2011).